Size effects on the Néel temperature of antiferromagnetic NiO nanoparticles

Natalia Rinaldi-Montes' , Pedro Gorria, David Martínez-Blanco, Antonio B. Fuertes, Inés Puente-Orench, Luca Olivi, and Jesús A. Blanco

Citation: AIP Advances **6**, 056104 (2016); doi: 10.1063/1.4943062
View online: http://dx.doi.org/10.1063/1.4943062
View Table of Contents: http://aip.scitation.org/toc/adv/6/5
Published by the American Institute of Physics

Size effects on the Néel temperature of antiferromagnetic NiO nanoparticles

Natalia Rinaldi-Montes,[1,a] Pedro Gorria,[2] David Martínez-Blanco,[3] Antonio B. Fuertes,[4] Inés Puente-Orench,[5] Luca Olivi,[6] and Jesús A. Blanco[1]
[1]*Departamento de Física, Universidad de Oviedo, E-33007 Oviedo, Spain*
[2]*Departamento de Física & IUTA, EPI, Universidad de Oviedo, E-33203 Gijón, Spain*
[3]*Servicios Científico-Técnicos, Universidad de Oviedo, E-33006 Oviedo, Spain*
[4]*Instituto Nacional del Carbón, CSIC, E-33080 Oviedo, Spain*
[5]*Instituto de Ciencia de Materiales de Aragón, CSIC-Universidad de Zaragoza and Institut Laue-Langevin, BP 156, F-38042 Grenoble Cedex 9, France*
[6]*Elettra-Sincrotrone Trieste S.C.p.A., 34149 Basovizza, Trieste, Italy*

(Presented 12 January 2016; received 6 November 2015; accepted 4 December 2015; published online 25 February 2016)

Among all antiferromagnetic transition metal monoxides, NiO presents the highest Néel temperature ($T_N \sim 525$ K). In this work, the size-dependent reduction of T_N in NiO nanoparticles with average diameters (D) ranging from 4 to 9 nm is investigated by neutron diffraction. The scaling law followed by $T_N(D)$ is in agreement with the Binder theory of critical phenomena in low-dimensional systems. X-ray absorption fine structure measurements link the decrease of T_N to the occurrence of size effects (average undercoordination, bond relaxation and static disorder) in the nearest and next-nearest Ni coordination shells that hold the key for the maintenance of the antiferromagnetic order. [http://dx.doi.org/10.1063/1.4943062]

In recent years, nanostructured antiferromagnetic (AF) materials have attracted a continuously increasing interest due to their promising applications as spin valves and next-generation magnetic random access memories (MRAM).[1] One of the hallmarks of nanomaterials is that their macroscopic physicochemical properties are strongly affected by size reduction, giving rise to a drastic modification of the magnetic behavior compared to their bulk counterparts'.[2,3] As a matter of fact, the magnetic configuration of atomic spins changes progressively as moving from the core, which usually presents a spin arrangement similar to that of the bulk material, to the surface, which exhibits a much higher magnetic disorder, leading to a plethora of glassy magnetic behaviors. The competition between surface and volume magnetic orders has been identified as a cause of high-field irreversibilities, high saturation fields, large coercivities and exchange bias effect.[4] In the case of cooperative phenomena such as ferromagnetism and antiferromagnetism, the decrease of the nanocrystal grain dimensions below the magnetic correlation length of the system results in the occurrence of strong fluctuations in the order parameter and the weakening of the exchange interactions.[5] Hence, the Curie (T_C) and Néel (T_N) order temperatures, which characterize the magnetic phase stability, present an intrinsic size dependence. While size variations of T_N have been exhaustively studied in thin films,[6] there are only a few published studies in nanoparticle (NP) systems. The majority of the experimental observations report on the reduction of T_N with decreasing NP diameter.[7–10] However, in order to confirm this trend further research should be geared into a wider scope of materials and NP sizes.

Nickel oxide constitutes a prototypical face-centered cubic (fcc) antiferromagnet, where Ni spins are coupled via the oxygen atoms by superexchange interactions and adopt a type-II spin arrrangement for $T < T_N$. Among all AF transition metal monoxides, NiO presents the highest

[a]Electronic mail: nataliarin@gmail.com

value of T_N (523 K). As a consequence, NiO can play a crucial role for addressing the challenge of storage density increase in magnetic recording media by allowing magnetic stability at very low volumes far above room temperature.[11] The current work presents a systematic study on how size reduction affects the Néel temperature of NiO NPs. In order to address this issue, neutron diffraction experiments have been carried out on NiO NPs with average sizes in the sub-10 nm range. This gives us direct information about the temperature dependence of the magnetization of each sublattice. The change of T_N as a function of the NP average diameter is discussed in the context of the Binder theory of critical phenomena in reduced dimension systems. In addition, x-ray absorption fine structure (EXAFS) measurements allow to correlate the reduction of T_N on decreasing NP size with the appearance of surface effects such as average undercoordination, bond relaxation and static disorder. We believe that knowledge about the size-dependent order temperatures of nanoscale AF materials may be used to advantage while designing future high-density storage memories based on magnetic proximity effects.

For this study, four samples of NiO NPs were produced using a one-pot method based on the pyrolysis of a Ni-nitrate taking place within a porous carbon matrix. The size of the NPs was controlled by means of the heating temperature, so that samples N4, N6, N7, N9 were prepared at 573, 613, 643 and 673 K, respectively. Further information about the synthesis details can be found elsewhere.[4] The procedure leads to NiO NPs with average diameters and standard deviations [D (σ)] of 4(1) [N4], 6(1) [N6], 7(1) [N7] and 9(1) [N9] nm, as derived from the fits to log-normal distributions of the size histograms created from transmission electron microscopy (TEM) micrographs [Fig. 1(a)]. High-resolution TEM (HRTEM) images [Fig. 1(b)], obtained under a 200 kV JEOL-JEM-2100F microscope, reveal the high crystal quality of the NPs, each one of them forming a single crystalline domain.

The microscopic magnetic structure of the NiO NPs was examined by unpolarized neutron diffraction (ND) at the Institut Laue-Langevin (Grenoble, France) on a two-axis powder diffractometer (D1B instrument) equipped with a high efficiency position sensitive detector. ND patterns in a q range of 0.4 - 4.4 Å^{-1} were collected at various temperatures between 10 K and 550 K at a neutron wavelength of λ = 2.52 Å. A double-walled vanadium cylinder sample holder was used to reduce neutron absorption. $Al_2Ca_3F_{14}Na_2$ and Si standards were measured in order to account for instrumental resolution. Analysis of the ND data was performed using the FullProf suite package based on the Rietveld method.[12] For the sake of comparison, the nuclear and magnetic crystal structures of a bulk NiO standard (Sigma Aldrich®, 99.999% trace metals basis) are first determined. For $T > T_N$ = 525(4) K, nuclear peaks can be fitted acording to a rocksalt $Fm\bar{3}m$ structure with a lattice constant of a = 4.187(2) Å at T = 550 K. When cooling to $T < T_N$, a set of magnetic reflections

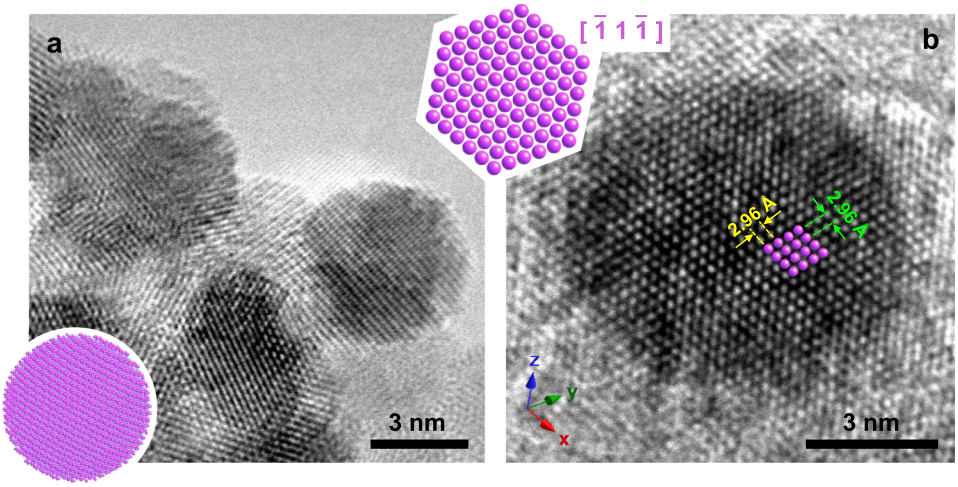

FIG. 1. (a) Representative TEM micrograph of sample N4. (b) HRTEM image of an individual NiO NP of sample N7 oriented along [$\bar{1}1\bar{1}$] direction. Lattice fringes of 2.96 Å correspond to (110) interplanar distance.

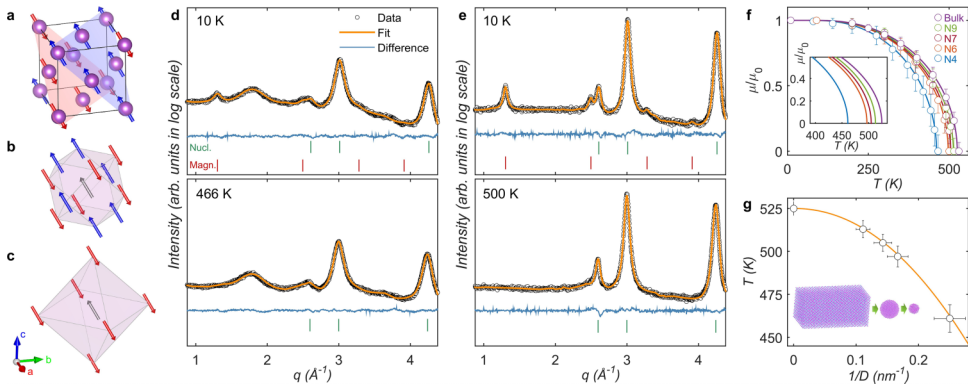

FIG. 2. (a) Magnetic structure of NiO. (b) Nearest-neighbor (Ni-1) and (c) next-nearest-neighbor (Ni-2) magnetic coordination shells. (d-e) ND patterns in logarithmic vertical scale of samples N4 (d) and N6 (e) for $T < T_N$ (top) and $T > T_N$ (bottom). (f) Temperature dependence of the normalized magnetic moment per Ni atom together with fits to Brillouin ($S = 1$) functions. Inset shows an enlarged view of the Néel temperatures of the samples. (g) NP size dependence of T_N. The continuous line is a fit to Eq. (1) (see text for details).

with half-integer indices arises, corresponding to type-II AF order in a fcc lattice. The full-profile fitting of the ND patterns corroborates the conventional order of NiO, namely, two magnetic sublattices, both with the spins oriented within (111) planes, but with the spins of one sublattice pointing in the $[11\bar{2}]$ direction and the spins of the adjacent sublattice antiparallel to it [Fig. 2(a)].[7] From the aforementioned magnetic structure, it can be derived that each Ni spin is surrounded by 12 nearest neighbors, the exchange interaction between them and the central spin being FM in sign for the 6 neighbors sitting on the same (111) plane and AF for the other 6 [Fig. 2(b)]. In addition, the next-nearest coordination shell consists of 6 spins antiferromagnetically alligned with respect to the central one [Fig. 2(c)]. In fact, the large AF exchage interaction between next-nearest neighbors is at the origin of the high Néel temperature of NiO compared to other AF transition metal monoxides.[13] At T = 10 K, the obtained magnetic moment per Ni atom of 2.0(2) μ_B corresponds to the spin-only value reported for bulk NiO, the orbital contribution being considered negligible in good approximation.[14]

Subsequent analysis of the ND patterns for NiO nanoparticulated samples [Figs. 2(d) and 2(e)] yields no significant differences between their magnetic structure and that of bulk NiO. Nevertheless, in a powder diffraction experiment performed with unpolarized neutrons, the large spin-incoherent scattering contribution coming from the water adsorbed on the surface of the NPs and the peak broadening due to the reduced size of the NPs make it difficult to detect subtle changes in the spatial orientation of the spins. Brok *et al.* have recently published a study on platelet-shaped NiO NPs (2.0 nm thick) where they overcome this problem by using polarized neutrons with XYZ-analysis. Their results evidence that Ni spins are tilted with respect to the primary (111) plane of the NPs by an angle of 30°. For all samples, the magnetic moment per Ni atom measured at T = 10 K coincides with that for the bulk NiO standard. However, when comparing the average crystallite diameter of the magnetic clusters (D_{mag}) with that of the nuclear ones (D_{nucl}), both obtained from the broadening of the magnetic and nuclear reflections, respectively, at T = 10 K, D_{mag} turns out to be significantly smaller than D_{nucl} for all samples. While D_{nucl} coincides with the previously estimated values from TEM size distributions [D_{nucl} = 4.2(2), 6.1(2), 7.3(3) and 8.9(1) nm for N4, N6 , N7 and N9, respectively], D_{magn} is between 0.6 - 1 nm smaller, irrespective of NP size [D_{nucl} = 3.6(3), 5.1(4), 6.5(4) and 8.0(3) nm for N4, N6 , N7 and N9, respectively]. This feature has been extensively observed in fine-particle systems and attributed to the random canting of spins at the NP surface due to the competition between the exchange and anisotropy energies.[2,5]

The temperature variation of the magnetic moment per Ni atom (μ) normalized by the T = 10 K value (μ_0) for the studied NiO samples is shown in Fig. 2(f). Assuming that the curves follow the theoretical Brillouin function for S = 1 systems, Néel temperatures of 461(8), 497(6), 505(5), 513(5) and 525(4) K are extrapolated for N4, N6, N7, N9 and the bulk standard, respectively. It is

well known that the order temperature of an AF material is severely altered in systems of reduced dimensionality. As the NP size approaches the magnetic correlation length of the system (ξ), the spin disorder at the NP surface spreads throughout the core of the NP, thus weakening the resultant exchange interactions and lowering the AF transition temperature. The dependence of T_N as a function of NP size is plotted in Fig. 2(g). As predicted by Binder theory of critical phenomena in low-dimensional systems,[15] our experimental data can be modeled by the following finite-size scaling law:

$$T_N(D) = T_N(\infty)\left[1 - \left(\frac{D}{\xi_0}\right)^{-1/\nu}\right] \quad (1)$$

where $T_N(\infty)$ is the Néel temperature for the bulk, ξ_0 is the magnetic correlation length of the system at $T = 0$ K and ν is a critical exponent related to ξ_0.[2] The best fit of our data to Eq. (1) [solid line in Fig. 2(g)] provides values of $\xi_0 = 1.4(6)$ nm and $\nu = 0.5(1)$, which are in good agreement with previous works reporting on critical phenomena in fine particle assemblies.

In order to gain further insights about how the breakage of the local symmetry in NPs affect the structural environment of surface atoms, EXAFS measurements were performed on the four samples of NiO NPs, together with the bulk NiO standard, at Elettra Synchrotron (Trieste, Italy) at the XAFS beamline (BL 11.1R). The spectra were collected around the Ni K-edge ($E_0 \sim 8333$ eV) at $T = 77$ K in transmission mode. The structural EXAFS signals were extracted from the absorption spectra using conventional procedures for background substraction and data normalization as implemented in the Athena software from IFFEFIT package.[16] Then, the fine structure, which extends from 25 to 1600 eV above the edge was converted to photon-electron wave vector k-space. The so derived EXAFS curves, $\chi(k)$ are displayed in Fig. 3(a). With the aim of obtaining direct information about the local structure around the Ni sites, the EXAFS signals were Fourier-transformed to radial units (R) in the range $2.4 < k < 20.5$ Å^{-1} and fitted to the EXAFS function in the $1.1 < R < 4.3$ Å interval in the direct R-space [Fig. 3(b)]:

$$\chi(k) = \sum_i \frac{N_i S_0^2 F_i(k)}{kR_i^2} exp(-2\sigma_i^2 k^2) exp\left[\frac{-2R_i}{\lambda(k)}\right] sin\left[2kR_i + \phi_i(k)\right] \quad (2)$$

The sum expands over all the backscattering atoms at the same distance R_i of the central atom, N_i and σ_i^2 being the number of i-th scattering neighbors and the Debye-Waller factor, respectively.[17] The backscattering amplitude and phase functions, $F_i(k)$ and $\phi_i(k)$, and the photoelectron mean free path, $\lambda(k)$, were theoretically generated from the FEFF6 code. A satisfactory agreement between experimental data and fits [solid lines in Fig. 3(b)] is achieved by including in the calculation the

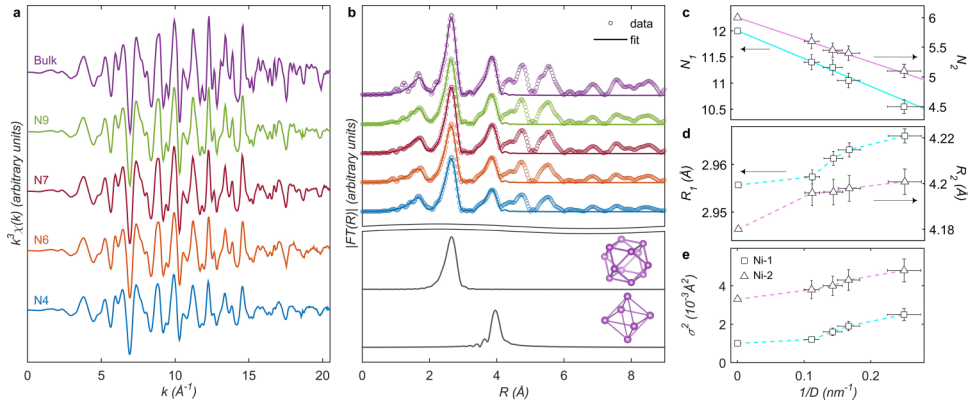

FIG. 3. (a) Ni K-edge EXAFS spectra measured at $T = 77$ K. (b) Experimental Fourier transforms (dots) and fits (lines) in the 1 Å $< R < 4.3$ Å region. At the bottom of the image, the single-scattering paths corresponding to Ni-1 and Ni-2 coordination shells are displayed. In (a) and (b) all the signals have been shifted up for the sake of comparison. (c-e) NP size dependence of the coordination numbers (c), interatomic distances (d) and Debye-Waller factors (e) associated to Ni-1 and Ni-2 coordination shells. The continuous lines in (c) are fits to Eq. (3). The dotted lines in (d) and (e) provide guides for the eyes.

scattering paths corresponding to O-1, Ni-1 and Ni-2 single scattering events and {O-1, Ni-2} and {O-1, Ni-2, O-1} multiple scattering paths. The value for $S_0^2 = 0.9$ was calculated starting from the NiO bulk standard and kept constant for the other samples, due to its high statistical correlation with N_i. Even though we will focus on the quantitative results corresponding to the Ni-1 and Ni-2 coordination shells [see bottom part of Fig. 3(b)], because of the key role that they play in the AF structure of NiO, it is worth noting that physically reliable parameters are obtained for all the scattering paths included in the fits.

As shown in Fig. 3(c), both the Ni-1 and Ni-2 coordination numbers present a continuous decrease on reducing NP size. This is due to the fact that surface Ni atoms are undercoordinated and that the recorded EXAFS signal is the average over all the Ni absorbing centres. Our results are in good agreement with the expected cluster size variation of the number of neighbors, given by:

$$N_i(D) = N_i(\infty)\left[1 - \frac{3}{2}\frac{R_i}{D} + \frac{1}{2}\left(\frac{R_i}{D}\right)^3\right] \quad (3)$$

where $N_i(\infty)$ is the coordination number for the bulk.[18] The lattice symmetry breaking experience by surface atoms also results in a relaxation of the Ni-1 and Ni-2 bond lengths, which becomes more pronounced as the average diameter of the NPs decreases [Fig. 3(d)]. Debye-Waller factors provide information about the dynamic (thermal agitation) and static (lattice distortion) disorder around the Ni atoms. Since all the measurements were carried out at $T = 77$ K, the increase of σ_i^2 with decreasing NP size [Fig. 3(e)] seems to be attributed to the static disorder originated from the more disordered environment that surrounds surface Ni atoms.

In summary, by using neutron diffraction the Néel temperatures of NiO NPs with average sizes between 4 and 9 nm have been determined. The observed scaling of T_N (D) is characteristic of phase transition in systems of reduced dimensionality. The lower average crystallite diameter of magnetic clusters compared to nuclear ones suggests the existence of a $\sim$ 0.5 nm thick layer of canted spins at the NP surface. Moreover, EXAFS analysis has allowed to correlate the drop of T_N on decreasing NP diameter with the appearance of size effects (undercoordination, bond relaxation and static disorder) in the volume-averaged Ni-1 and Ni-2 coordination shells, which are responsible for maintaining the AF order of NiO up to a temperature higher than any other AF transition metal monoxide.

N. Rinaldi-Montes gratefully acknowledges doctoral grant FPU12/03381 from the Ministerio de Educación, Cultura y Deporte (MECD). This work was financially supported by research projects MAT2011-27573-C04 (MINECO, Spain) and FC-15-GRUPIN14-037 (Asturias Government, Spain).

[1] G. A. Prinz, Science **282**, 1660 (1998).
[2] X. Batlle and A. Labarta, J. Phys. D: Appl. Phys. **35**, R15 (2002).
[3] N. Rinaldi-Montes, P. Gorria, D. Martínez-Blanco, A. B. Fuertes, L. Fernández Barquín, J. Rodríguez Fernández, I. de Pedro, M. L. Fdez-Gubieda, J. Alonso, L. Olivi, G. Aquilanti, and J. A. Blanco, Nanoscale **6**, 457 (2013).
[4] N. Rinaldi-Montes, P. Gorria, D. Martínez-Blanco, A. B. Fuertes, L. Fernández Barquín, I. Puente-Orench, and J. A. Blanco, Nanotechnology **26**, 305705 (2015).
[5] S. Mørup, D. E. Madsen, C. Frandsen, C. R. H. Bahl, and M. F. Hansen, J. Phys.: Condens. Matter **19**, 213202 (2007).
[6] X. Y. Lang, W. T. Zheng, and O. Jiang, Phys. Rev. B **73**, 224444 (2006).
[7] E. Brok, K. Lefmann, P. P. Deen, B. Lebech, H. Jacobsen, G. J. Nilsen, L. Keller, and C. Frandsen, Phys. Rev. B **91**, 014431 (2015).
[8] S. N. Klausen, P. A. Lindgård, K. Lefmann, F. Bødker, and S. Mørup, Phys. Status Solidi A **189**, 1039 (2002).
[9] I. V. Golosovsky, I. Mirebeau, G. André, M. Tovar, D. M. Tobbens, D. A. Kurduykov, and Y. A. Kumzerov, Phys. Solid State **48**, 2130 (2006).
[10] M. Molina-Ruiz, A. F. Lopeandía, F. Pi, D. Givord, O. Bourgeois, and J. Rodríguez-Viejo, Phys. Rev. B **83**, 140407(R) (2011).
[11] J. A. De Toro, D. P. Marqués, P. Muñiz, V. Skumryev, J. Sort, D. Givord, and J. Nogués, Phys. Rev. Lett. **115**, 057201 (2015).
[12] J. Rodriguez-Carvajal, in *Satellite Meeting on Powder Diffraction of the XV IUCr Congress* (1990), p. 127.
[13] M. T. Hutchings and E. J. Samuelsen, Phys. Rev. B **6**, 3447 (1972).
[14] W. Roth, Phys. Rev. **110**, 1333 (1958).
[15] K. Binder, Physica **62**, 508 (1972).
[16] B. Ravel and M. Newville, J. Synchrot. Radiat. **12**, 537 (2005).
[17] M. A. Peck and M. A. Langell, Chem. Mater. **24**, 4483 (2012).
[18] S. Calvin, M. M. Miller, R. Goswami, S. F. Cheng, S. P. Mulvaney, L. J. Whitman, and V. G. Harris, J. Appl. Phys. **94**, 778 (2003).